Hindawi
Mathematical Problems in Engineering
Volume 2022, Article ID 7027528, 15 pages
https://doi.org/10.1155/2022/7027528

Research Article

Analysis on Vibroacoustic Fatigue Life of Empennage in a Hypersonic Vehicle

Wang Hongxian,[1] **Zhang Ming**,[2] **and Nie Hong**[2]

[1]*Nanjing University of Aeronautics and Astronautics, Nanjing 210016, China*
[2]*State Key Laboratory of Mechanics and Control of Mechanical Structures, Nanjing University of Aeronautics and Astronautics, Nanjing 210016, China*

Correspondence should be addressed to Wang Hongxian; whx915@nuaa.edu.cn

Received 18 April 2022; Accepted 14 June 2022; Published 23 August 2022

Academic Editor: Wei Liu

In this study, the fatigue life prediction in hypersonic vehicle noise environment is researched under the structural vibration caused by the engine jet noise and the aerodynamic noise. A finite element analysis model is first established, and then natural frequency and vibration mode are obtained. According to the modal analysis, the vibroacoustic coupling calculation is finished in the dynamic analysis software. Modal participation factor, modal displacement, and the power spectral density of the stress response on the coupled surface are acquired. The finite element, border component, and vibrating stress analytical techniques are also employed in this research to predict the acoustical fatigue performance of the tail fins of a specific type of spacecraft. On the basis of vibration fatigue theory, identified material S–N curve, and linear cumulative damage theory, the Dirlik model in the frequency domain method for vibration fatigue is used to predict the fatigue life of empennage. According to the characteristics of the acoustic load, effects of the load characteristics, and damping ratios on the fatigue conditions, the design of the antifatigue design is put forward.

1. Introduction

Hypersonic aircrafts are subjected to high-frequency vibration loads during flight, and these loads are mainly caused by the jet noise of the engine propulsion system and the aerodynamic noise in the flight mission. The energy of the strong noise in the atmosphere and body of the hypersonic flight engine are far more than those in an ordinary aircraft. The positions near the engine in high strong parts, such as the engine combustion chamber and tail skin, are prone to increasing fatigue problems. When the sound pressure level of the surface of the aircraft exceeds 130 dB, the structural components are subject to high-intensity noise fluctuations that cause the occurrence of resonance or forced vibration, which generates stress brought by structural damage. The sound sensitive equipment in the cabin may also be greatly affected [1]. Hypersonic vehicles move quickly greater than five times the sound speed, enabling a new category of aircraft vehicles capable of providing quicker space travel, extensive military reaction, and economic airline travel. The body frame, body temperature defense system, fuel storage, and wings layout are the main components. Studying the sonic fatigue of the position at high sound intensity is important. However, the cost of the noise test is often high, the design cycle is long, and the test procedure is complicated. Therefore, research on the acoustic load response and the acoustic fatigue calculation technology of aircrafts must be increasingly conducted [2, 3]. The nonlinear combination between such a high frequencies ultrasound waves and a much shorter wavelength structure motion is used in the Vibroacoustic Modulation technique. The nonlinear surfaces are where this interaction occurs. It monitors fatigue and stress-corrosion damage development in metal using in-plane nonresonance extremely lower frequencies tension vibrations [4].

A novel optimization framework on the basis of a multidisciplinary optimization procedure is applied to the vibroacoustic finite element method (FEM) model of an aircraft fuselage mock-up [4–6]. The current frequency domain methods then simulated the analogue spectrum and selected three materials for comparison in the different frequency domain methods [7, 8]. A random vibration fatigue life estimation of the sample method was proposed through the method with spectral density to describe the characteristics of the wide band random vibration. Several factors of vibration fatigue were also studied. By conducting the time-domain simulation to the power spectral density, the distribution function of loaded rainfall amplitude was obtained, and the vibration fatigue life of the structural was calculated [7, 8]. The modal analysis of the whole state of a certain aircraft in a free state was carried out, and the random vibration response analysis of the structure under aerodynamic noise was performed. Good results were obtained and compared with the experimental results. The fatigue life formula under narrowband random vibration was deduced. Based on the study of differently shaped power spectral density (PSD) correction results and Dirlik, the fatigue life estimation formula for broadband random load was established in 2005 [6, 9]. A Power Spectral Density (PSD) is a metric that compares the power level of a transmission to its wavelength. Broadband randomized events are often described using a PSD. The spectral resolution used to encode the data normalizes the PSD's loudness [10]. Although the sound fatigue problems of the engine and the inlet were widely analyzed in existing literature, research on the sound fatigue of the tail, the fuselage, and the wing in the hypersonic environment is scarce. The vibration fatigue caused by noise load in hypersonic environment was investigated in this study.

2. Main Research Content and Methods

Based on an aerospace plane, this study focuses on the sound–vibration coupling phenomenon of the lightweight V-tail under the engine take-off noise environment; it also estimates the sound fatigue life on the basis of the structural dynamic response obtained from the sound–vibration coupling analysis. On this basis, several influencing factors of acoustic fatigue are proposed, and a set of more complete acoustic fatigue life prediction schemes are summarized. The main research contents of this article include the following:

(1) Modal analysis based on FEM.

(2) Acoustic–vibration coupling calculation based on modal.

(3) Acoustic fatigue calculation based on dynamic response.

(4) Research on the influencing factors of acoustic fatigue.

The objective of dynamic analysis in structural mechanics would be to identify an object's or structure's inherent dynamic characteristics and energies under simple vibration. A physical object can also be tested to identify its native frequency and modulus. Acoustic fatigue is a condition that occurs when pipework is subjected to excessive tension as a result of excessive noise. High sound at pressures lowering devices like pressure regulator or limitation holes stimulates downstream pipeline, causes piping shaking, and puts a great deal of stress upon that branches or welded support.

2.1. Method of Fatigue Life under Sound Vibration Judge Coupling. A coupling coefficient (λ_c) can be used to determine whether the coupling action must be considered in the coupling problem [11]. Many unfavorable events can occur from sonic coupling between the components of a microarray transducer. Coupling coefficients are generated through lateral mode creation in the components and also surfaces and lamb waves in the backup and front corresponding levels.

$$\lambda_c = \frac{\rho_0 c}{\rho_t T \omega}, \tag{1}$$

where ρ_0 is the density of the fluid, c is the velocity of the sound in the fluid, ρ_t is the density of the structure, T is the equivalent thickness of the structure, and ω means the angular frequency.

For the acoustic field under the action of random sound field, the range of angular frequency is large, with which the coupling effect is obvious in the data calculation. Therefore, the coupling effect should be considered. The stress response of the structure under the acoustic load is studied. Considering the characteristics of the sound load, the sound field of the model is simulated.

2.2. Definition of the Coupling Surface. For structural and acoustic grids, establishing a data transfer to present a coupling relationship is necessary. Similarly, defining the mapping relationship between both grids is important [12]. Given that nodes and units between different types of grids are not one-to-one, the mapping between grids must be defined. The coupling between the structure and the fluid medium does not exist entirely on the whole structure. In this case, defining a coupling surface is necessary to well simulate the real situation. The process of defining the coupling surface actually implements the transfer process between the grid data. The mapping algorithm includes the node number, maximum distance, element maximum distance, and conservative maximum distance. For the maximum distance algorithm, also defined as the number of influence nodes or maximum distance, the value of the target node is determined by the value of the source node, as in Figure 1. The specific formula is as follows:

$$P_{\text{Target}} = \frac{\sum_{i=1}^{N} \left(P_i^{\text{Source}}/d_i\right)}{\sum_{i=1}^{N} \left(1/d_i\right)}, \tag{2}$$

where P_{Target} refers to the target—the value of the node; d_i is the radius; P_i^{Sourse} is the value on the source node.

To decouple the kinetic equation represented by the physical coordinates, switching to the modal coordinate

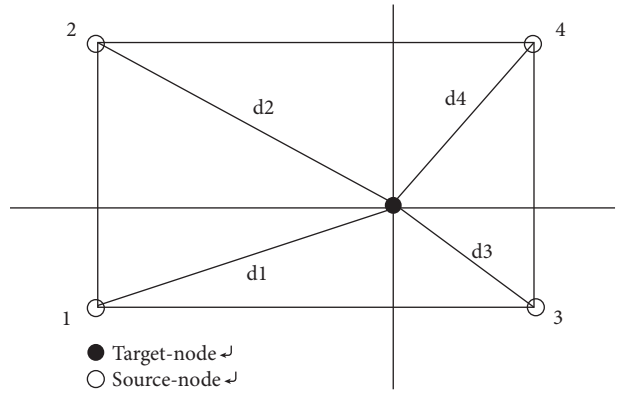

Figure 1: Diagram of data transfer.

system is necessary. According to the orthogonality of the eigenvector, the modal matrix, modal mass, modal stiffness, modal damping, and modal coordinates can be defined separately [13]. The vibration displacement can be written as follows:

$$\{u\} = \eta_1\{\phi_1\} + \eta_2\{\phi_2\} + \cdots + \eta_n\{\phi_n\} = \Phi\{\eta\}, \tag{3}$$

where $\{\eta\} = \begin{pmatrix} \eta_1 \\ \eta_2 \\ \vdots \\ \eta_n \end{pmatrix}$ is a vector of modal participation factors η_r.

Through the above transformation, the original coupling of the kinetic equation into the decoupled modal coordinate system under the modal equation is

$$M_r\ddot{\eta}_r + C_r\dot{\eta}_r + K_r\eta_r = F_r, \quad r = 1, 2, \ldots, n. \tag{4}$$

By solving the kinetic equation of n independent modal coordinates represented by the above equation, we can obtain the modal participation factor corresponding to the modal coordinates under modal coordinates, including the displacement response of the system in the physical coordinate system. The dynamic response of the system is superimposed by the modal response of each order. The modal participation factor indicates the proportion of the modes in the total response. The participation factor is only related to the system structure parameters and has nothing to do with the disturbance.

2.3. Model of Fatigue Life Estimation. The frequency domain method is used to describe the stress information of the stochastic process with the spectral parameters of the response power spectral density. Then, the S–N curve and fatigue cumulative damage theory are used to calculate the life.

Regarding the random process for various states, a statistical function of the sample function can be used to describe the statistical characteristics of the entire process [13]. In general, the environmental vibration of an aircraft has a steady state of various properties. The first-order amplitude probability density function is defined as

$$p(q_i) = \lim_{\Delta q_i \longrightarrow 0}\left[\lim_{T \longrightarrow \infty}\frac{1}{T}\sum_{i=1}^{\infty}\Delta t_i\right]. \tag{5}$$

According to Miner linear damage theory, the structure is due to the stress cycle of different stress levels. The total fatigue damage of the structure is

$$D = \sum D_i = \sum \frac{n_i}{N_i}, \tag{6}$$

where the stress level is expressed, indicating the corresponding fatigue life at the stress level. In a certain time T, the stress range in the number of cycles is

$$n_i = \nu T p(S_i)\Delta S_i, \tag{7}$$

where ν is the number of stress cycles per unit time, and $p(S_i)$ is the probability density function of stress amplitude.

The time of fatigue damage can be obtained using the following:

$$D = \nu T \int_0^{\infty} \frac{p(S)}{N(S)}\mathrm{d}S. \tag{8}$$

According to the fatigue damage criterion, the structure is destroyed, and the fatigue life is

$$N_T = \frac{1}{\nu \int_0^{\infty} (p(S)/N(S))\mathrm{d}S}. \tag{9}$$

The fatigue life of the structure depends on the stress response density. The broadband distribution method is used to calculate the probability density of the rain flow amplitude.

Dirlik's Monte Carlo time-domain simulation is conducted to study the power spectral density function of different shapes. Four inertia moments are used to describe the amplitude density function. The velocity or path of moving object is controlled by four inertial moments. The ability of items to continue travelling in a single direction at a constant pace when no pressures occur on them would be one example of this feature. Both a translational and a rotating component may be present in the averaged movement [14].

$$p(S) = \frac{(D_1/Q)e^{(-Z/Q)} + \left(D_2 Z/R^2\right)e^{\left(-Z^2/2R^2\right)} + D_3 Z e^{\left(-Z^2/2\right)}}{2\sqrt{m_0}}, \tag{10}$$

where 0 is the order spectrum moment.

$$\begin{aligned} D_1 &= \frac{2\left(\chi_m - \gamma^2\right)}{1+\gamma^2}, \\ D_2 &= \frac{1-\gamma^2-D_1+D_1^2}{1-R}, \\ D_3 &= 1 - D_1 - D_2, \\ Z &= \frac{S}{2\sqrt{m_0}}, \\ Q &= \frac{1.25\left(\gamma - D_3 - D_2 R\right)}{D_1}, \\ R &= \frac{\gamma - \chi_m - D_1^2}{1-\gamma-D_1+D_1^2}, \\ \gamma &= \frac{m_2}{\sqrt{m_0 m_4}}, \\ \chi_m &= \frac{m_1}{m_0}\sqrt{\frac{m_2}{m_4}}. \end{aligned} \tag{11}$$

The noise signal of the aircraft is a high-frequency broadband random signal. The Dirlik model is simple, fast, and suitable for wideband signal.

2.4. Average Stress Correction. In different stages of life, the effect of average stress is not the same; for different materials, the effect of average stress is also not the same. To consider the effect of average stress on fatigue life, especially the high-cycle fatigue life, Gerber et al. proposed different correction methods. Meanwhile, Goodman proposed a revised method.

Goodman's mean stress correction equation is as follows:

$$\frac{S_a}{S_e} + \frac{S_m}{S_u} = 1. \tag{12}$$

S_a is the stress amplitude, S_m is the average stress, S_e is the symmetrical cyclic stress, and S_u is the strength limit. Goodman's formula, especially in the fatigue limit, has a small error in processing the average tensile stress.

2.5. Process of Fatigue Life Analysis. Process of fatigue life analysis is shown in Figure 2.

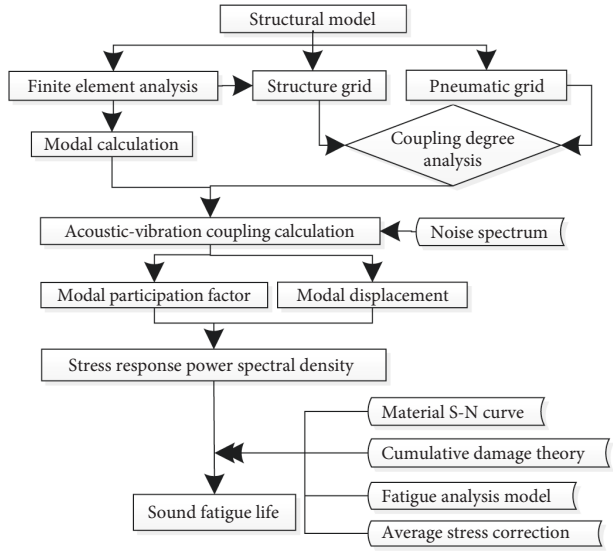

Figure 2: Process of fatigue life analysis.

3. Acoustic–Vibration Coupling Analysis Based on Modal

3.1. Modal Analysis Based on FEM

3.1.1. Establishment of FEM. Taking the left side of the tail of a type of spacecraft as the object of study, the CAD diagram of the tail model is established in Figure 3.

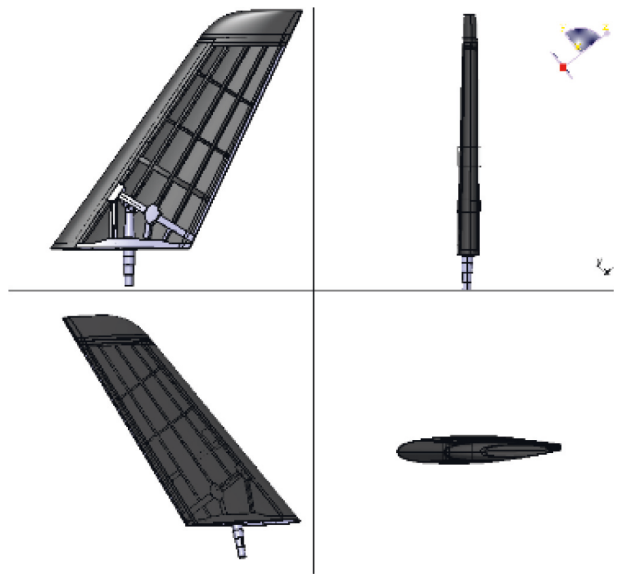

Figure 3: CAD diagram of a tail model.

The FEM of the tail fin is also established. With geometric cleanup, geometric simplification, topological restoration, and topological improvement, the resulting simplified FEM is shown below (skin hiding) in Figure 4.

3.1.2. Division of 2D Grid and Boundary Constraints. To facilitate the analysis of sound and vibration, the structural meshing should be consistent with the acoustic grid, that is, to meet the requirements in the acoustic simulation software for grid size. In the analysis of dynamic software, sound reflection and diffraction and refraction effects are considered [15]. The grid size is too large and may lead to a great error in the accuracy of the calculation results. For a linear finite element and a boundary element model, at least six cells in a minimum wavelength and at least three units for

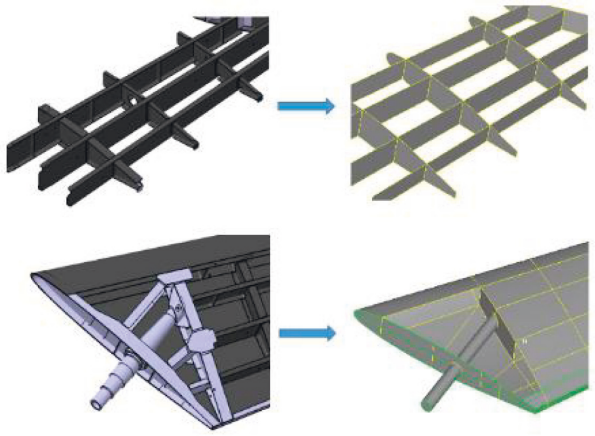

Figure 4: Simplified model of geometric relationships.

the quadratic unit are assumed. Given that the linear unit is used here, assuming that the propagation speed of sound is c and the highest frequency is $f_{\max}$, the unit length L which was divided should meet the following conditions [16]:

$$L \leq \frac{c}{6 f_{\max}}. \tag{13}$$

In this study, the fluid medium is air, the speed of sound is 340 m/s, the maximum frequency calculated is 4000 Hz, and element length $L \leq 14.2$ mm is obtained by substituting the formula. The 14 mm size is selected as the grid standard size to be divided. The divided grid cells are illustrated in Figure 5.

The meshing adopts quadrilateral elements as the main method and triangular elements as the auxiliary method, which not only ensures the calculation accuracy, but also considers the calculation speed. The final divided mesh unit is shown in Figure 5. The full tail model is divided into 19366 meshes and 18037 nodes.

Select the mesh node at the end as the slave node, the master node is automatically obtained through the geometric relationship, constrain the first 5 degrees of freedom of the master node, and release the sixth degree of freedom, that is, the rotation degree of freedom around the rudder axis in Figure 6.

3.1.3. Setting of the Material and Grid Properties. Four main materials are used: T300/603A, T300/603A, TC4, and 30CrMnSiA, as displayed in Figure 7. Thickness of tail wing parts is given in Table 1.

3.1.4. Performance of Modal Analysis. As the maximum external excitation frequency of 4000 Hz, the frequency range of the solution modal control is 1–6000 Hz, the modal solution, to ensure the accuracy of the results and consider the calculation cost at the same time.

3.1.5. Modal Analysis Results. Table 2 shows the natural frequency of the model as a whole. The range of the natural frequency values of the first-order to the 900-

Figure 5: Grid division.

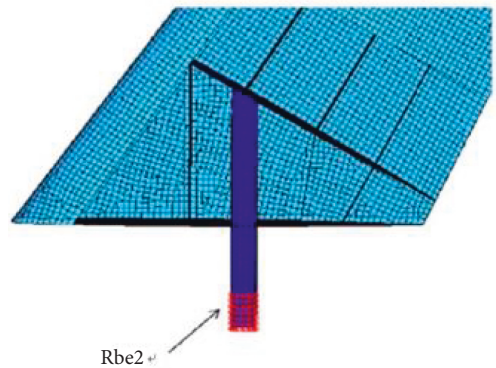

Figure 6: Grid division.

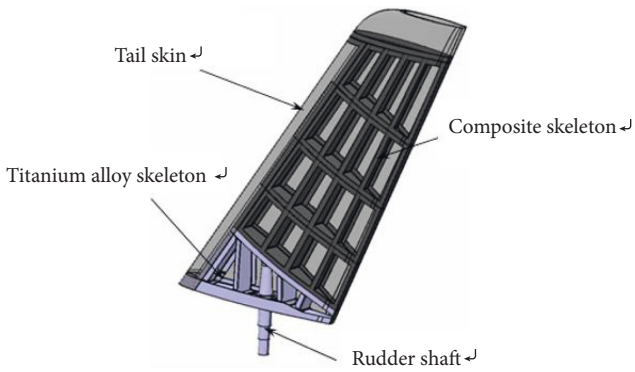

Figure 7: Material of the wing components.

Table 1: Thickness of tail wing parts.

Numbering	Name	Material	Thickness (mm)
1	Skin	2A14	2.2
2	Rudder shaft	30CrMnSiA	10
3	Ribs	T300/603A	1.5
4	Side ribs	TC4	10
5	Trailing edge	T300/603A	3
6	Wall	T300/603A	3
7	Beam	TC4	4
8	Reinforced ribs	TC4	12

Table 2: Natural frequency.

Modal order	Natural frequency (Hz)
1	33.5774
2	36.7333
3	153.0123
4	208.4317
5	397.1541
⋮	⋮
31	1012.5375
⋮	⋮
153	2004.5829
⋮	⋮
495	4005.2000
⋮	⋮
900	6000.4287

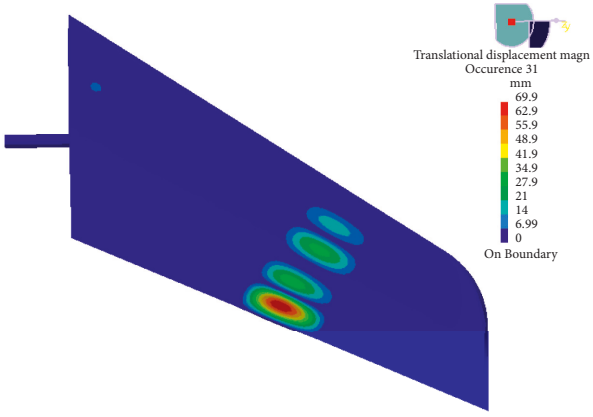

Figure 8: Order mode.

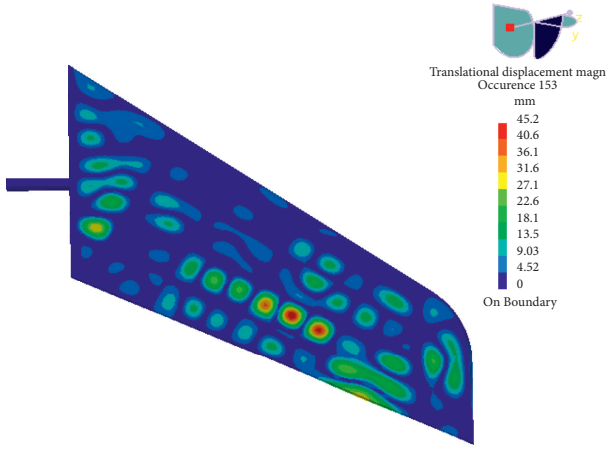

Figure 9: 153rd order mode.

order modes of the model is 33.5774–6000.4287 Hz. The table also presents the natural frequency values for several typical orders.

3.1.6. Modal Vibration Mode. In this study, the excitation is the acoustic load, and the frequency is high. Therefore, the high-order mode should be calculated while studying the low-order mode. In Figures 8–11, high-end mode selections

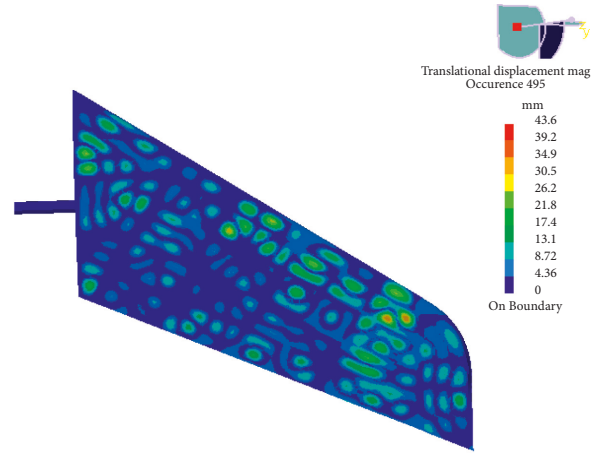

Figure 10: 495th order mode.

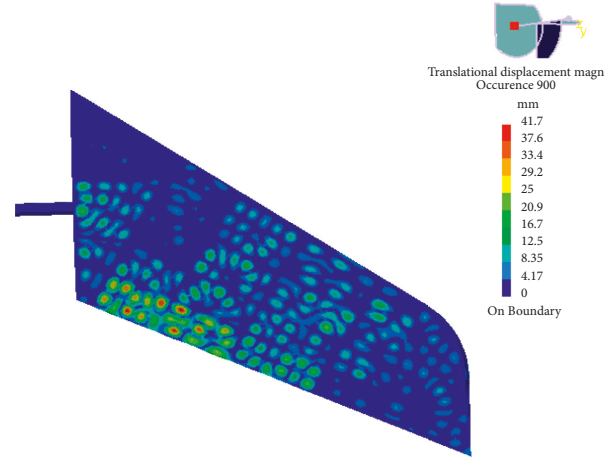

Figure 11: 900th order mode.

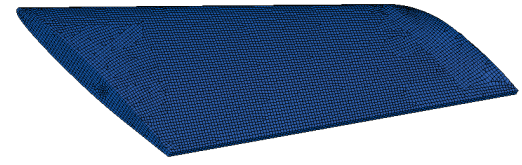

Figure 12: Acoustic grid.

31, 153, 495, and 900 correspond to the natural frequency values of 1000, 2000, 4000, and 6000 Hz.

3.2. Acoustic Coupling Calculation. Importation of structure grid, modal, and acoustic grid ware: Acoustic grid involvement is a valuable diagnostic technique for determining which areas of a building contribute considerably to the internal acoustics. Modal analysis aids in determining the vibration signals of a physical building component by displaying the activity of various portions of the building under dynamic loads, including those caused by electrostatic controllers' lateral loads [10]. Grid ware is constantly looking for changes that may affect the grid's overall performance.

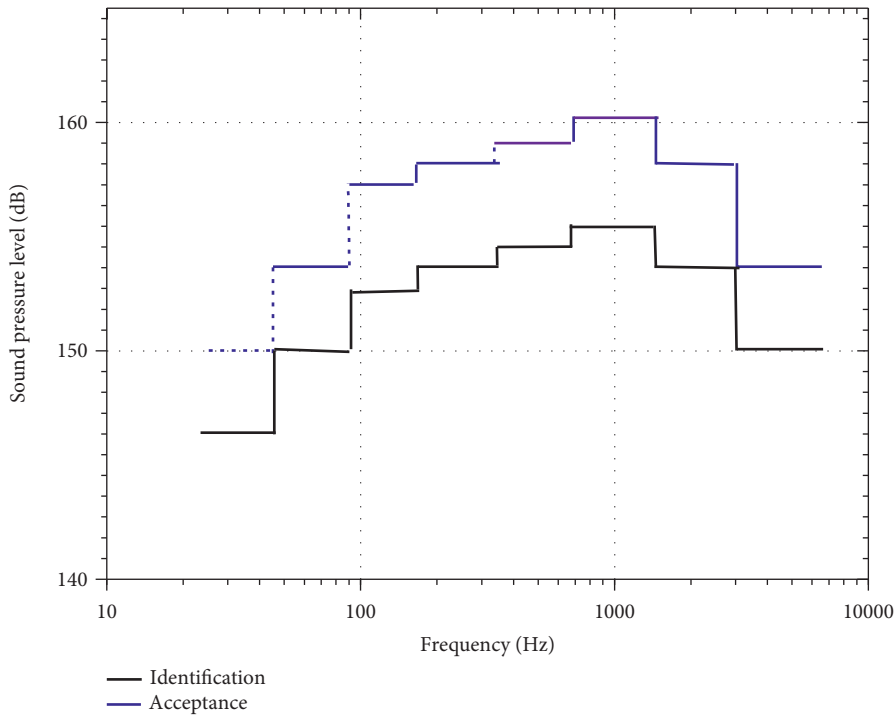

Figure 13: Noise spectrum.

The technology identifies defects earlier and in live time, allowing you to arrange rapid adjustments and respond quickly to acoustics emergencies. With the boundary element method used for acoustic numerical calculation, the structure grid, acoustic grid, and structure modal are imported. Acoustic grid panels have a tiling pattern that aids in the absorbing of reflecting waves, allowing audio to be clarified and improved in a space. Because of their size, those screens are good for treating vast areas of a space at the same time. The grid of the analysis structure uses the modal analysis grid. The acoustic grid is divided by a 2D grid. The envelope surface of the structure is first adopted, and then the surface mesh on the envelope surface is divided. To ensure that the structure grid and the acoustic grid have a good correspondence, the standard size is calculated, and the selected acoustic grid size is 14 mm.

Definition of sound load: The external sound load data are obtained from the measured sound pressure level spectrum, as shown in Figure 12. The acceptance test and the identification test sound pressure level spectrum correspond to the solid part and the broken line part in Figure 13. The experiment time is one and three minutes, respectively [16]. The given spectrum is octave, the frequency of each center band is twice the frequency of the center band of the previous band, and the sound pressure level corresponding to each center band is read and tabulated as in Table 3.

Definition of the sound source for the random diffusion of the sound field and the determination of the sound field of the sound pressure distribution by the spectrum [17]: A noise spectrum is the given data in Table 4. Thus, the sound pressure level must be converted to sound pressure to obtain the sound pressure spectrum [18]. The conversion formula is

Table 3: Noise acceptance test sound pressure level spectrum.

Center frequency (Hz)	Sound pressure level within octave bandwidth (dB)	
	Acceptance level	Appraisal level
31.5	146	150
63	150	154
125	153	157
250	154	158
500	155	159
1000	156	160
2000	154	158
4000	150	154

Table 4: Sound pressure spectrum.

Center frequency (Hz)	Sound pressure level (dB)	Sound pressure effective value (Pa)
31.5	150	632.4
63	154	1002.4
125	157	1415.9
250	158	1588.7
500	159	1782.5
1000	160	2000
2000	158	1588.7
4000	154	1002.4

$$p_e = p_{\text{ref}} \times 10^{\left(L_p/20\right)}. \tag{14}$$

Definition of the sound load concept and the selection of an idealized distribution of the reverb distribution: In the space where the diffuse sound field is satisfied, the sound

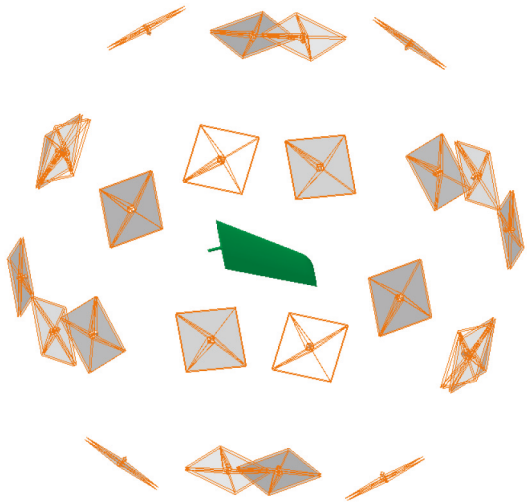

Figure 14: Sound pressure distribution.

Figure 15: Coupling surface.

field distribution statistics of each point are uniform everywhere, and the acoustic energy probability from each direction is the same. To achieve these conditions, fully reflecting the various walls of sound waves is necessary. The 24 unrelated plane waves, evenly distributed in the structure of the spherical sphere, are defined. The spherical radius is obtained using the algorithm automatically in Figure 14.

3.2.1. Definition of the Coupling Surface. The surface skin of the V-tail is in direct contact with the sound field, and the equivalent thickness of the skin is minimal. Therefore, the contact surface between the skin and the sound field is a strongly coupled region, so that all external skin grids are selected in addition to the control rudder shaft. The corresponding sound field grid is defined as the coupling surface in Figure 15.

3.2.2. Definition of the Coupling Surface. In this study, the acoustic excitation is reduced to 24 plane waves, which are equivalent to 24 irrelevant excitation conditions. Under different operating conditions, the software calculates the participation factors of the modal modes. Here are a few typical equations in the first modal participation factor schematic in Figures 16 to 19.

In contrast to the natural frequency table, all modal participation factors have a maximum value near their corresponding natural frequency. For example, the seventh-order modal participation factor is maximized at a frequency of approximately 500 Hz. The seventh-order mode has the largest proportion of the total response caused by the external excitation at a frequency of 500 Hz.

3.2.3. Displacement Response Result. In this study, the acoustic load spectrum is the octave spectrum; thus, the frequency range is 31.5–4000 Hz, and the incremental step is octave increment; that is, the frequency of the latter step is twice as long as the previous step. This section gives the displacement response under all the calculated frequency excitations under Principal Component 1. As the excitation frequency increases, the displacement response of the structure becomes more complex, and the response amplitude becomes smaller in Figure 20.

3.3. Stress Response. The response of the structure under the action of each plane wave is calculated. In this section, the response of the random response is calculated using the coupling response. Given that the defined plane waves are irrelevant and the coefficient of the participation of Principal Component is 1, it is a unit diagonal matrix. The response of each plane wave is synthesized. A random response of the random field is calculated, and all the nodes on the coupling surface are chosen to calculate the stress response. The stress response can be obtained from the power spectral density. Figures 21 and 22 illustrate the stress and power spectral density of the x and y directions of the mesh cell number 8755; the z-stress in the 2D element is zero. Many peaks can be seen in the stress response power spectral density, which indicates that the structural vibration is caused by multimode superposition, and the structural response is expressed as wideband multimodal.

4. Sound Fatigue Calculation

4.1. Stress–Life Curve. The typical stress–life curve (S–N curve) can be divided into three segments: low-cycle fatigue zone, high-cycle fatigue zone, and subfatigue zone. When the external load stress is less than the fatigue limit (i.e., infinite life), in general, take N, which is equal to the corresponding stress value. When the stress is equal to the tensile strength of static tension, the life is a stretching time; in the subfatigue zone, the S–N curve in the logarithmic coordinate system is almost a straight line. In a fatigue analysis, S stands for the stress range that is used to compute the deterioration [19, 20]. It is useful to determine the number of required cycles till a material fails, but it does not tell you how much fatigue damages the materials before the material fails.

Access to information obtained 2A14 aluminum alloy tensile strength $\sigma_b = 440$ MPa; the fatigue limit $S_{ae} = 130$ MPa. Use the power function formula:

$$S^{\alpha}N = C. \tag{15}$$

On both sides of the above pairs of logarithms,

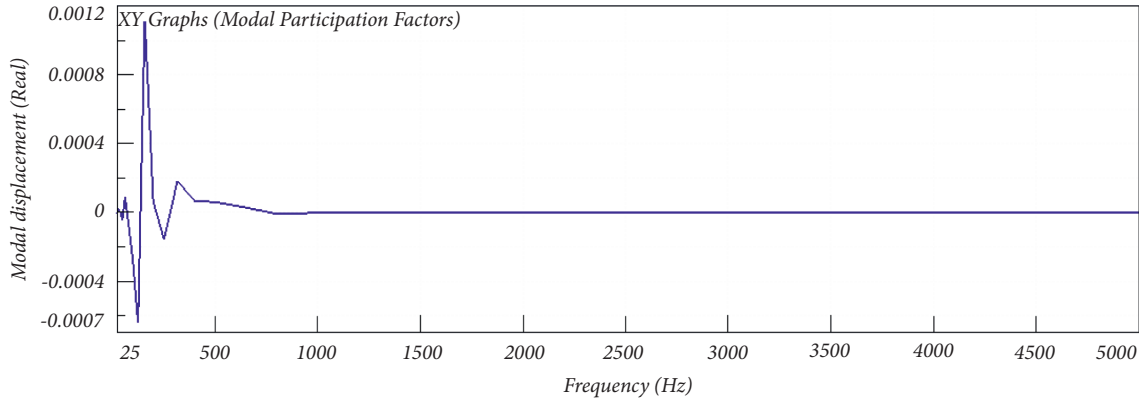

Figure 16: Participation factor of the third-step modal.

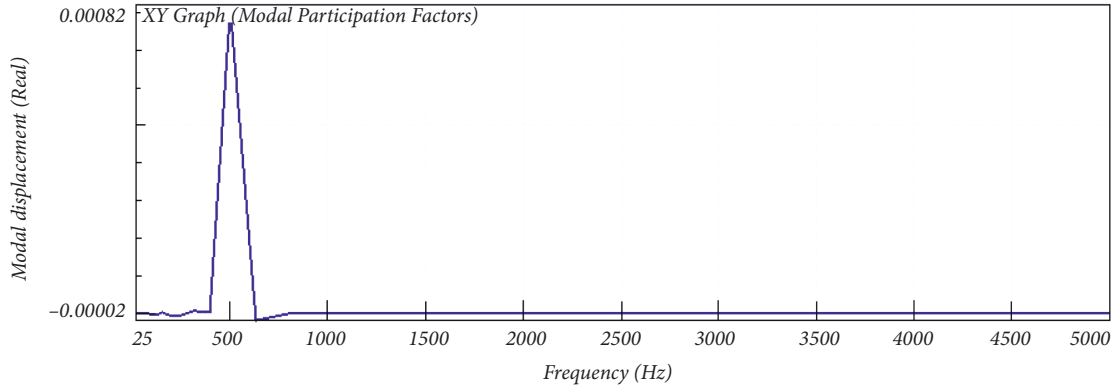

Figure 17: Participation factor of the seventh-step modal.

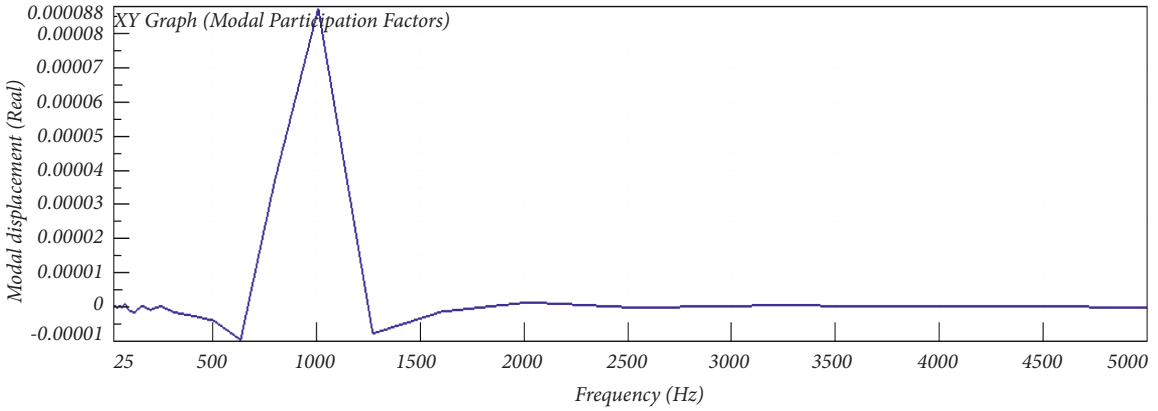

Figure 18: Participation factor of the thirty-first-step modal.

$$\lg N = a + b\lg S, \tag{16}$$

where a and b are the material constants, and the empirical formula of the S–N curve of the power function is a straight line on the double logarithmic plot [21].

By studying the effect of loading frequency on the fatigue life curve of metal materials, their loading frequency has little effect on the S–N curve when the metal materials only undergo elastic deformation, as shown in Figure 23. In this study, the fatigue life curve is calculated by static fatigue.

4.2. Fatigue Life Analysis Theory. This research chooses Miner linear superposition theory.

The fatigue life estimation method of Dirlik model is adopted. The frequency domain method is used to describe the stress information of the stochastic process with the

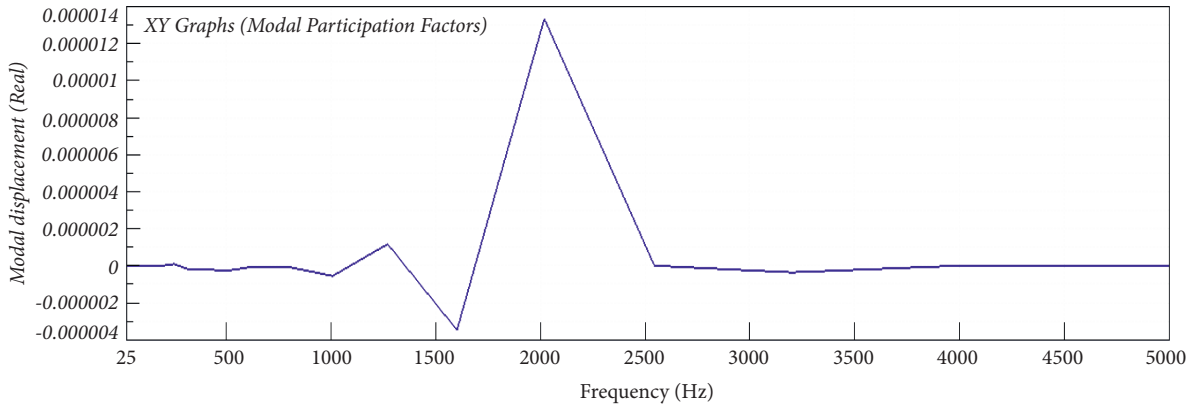

Figure 19: Participation factor of the one hundred and fifty-third-step modal.

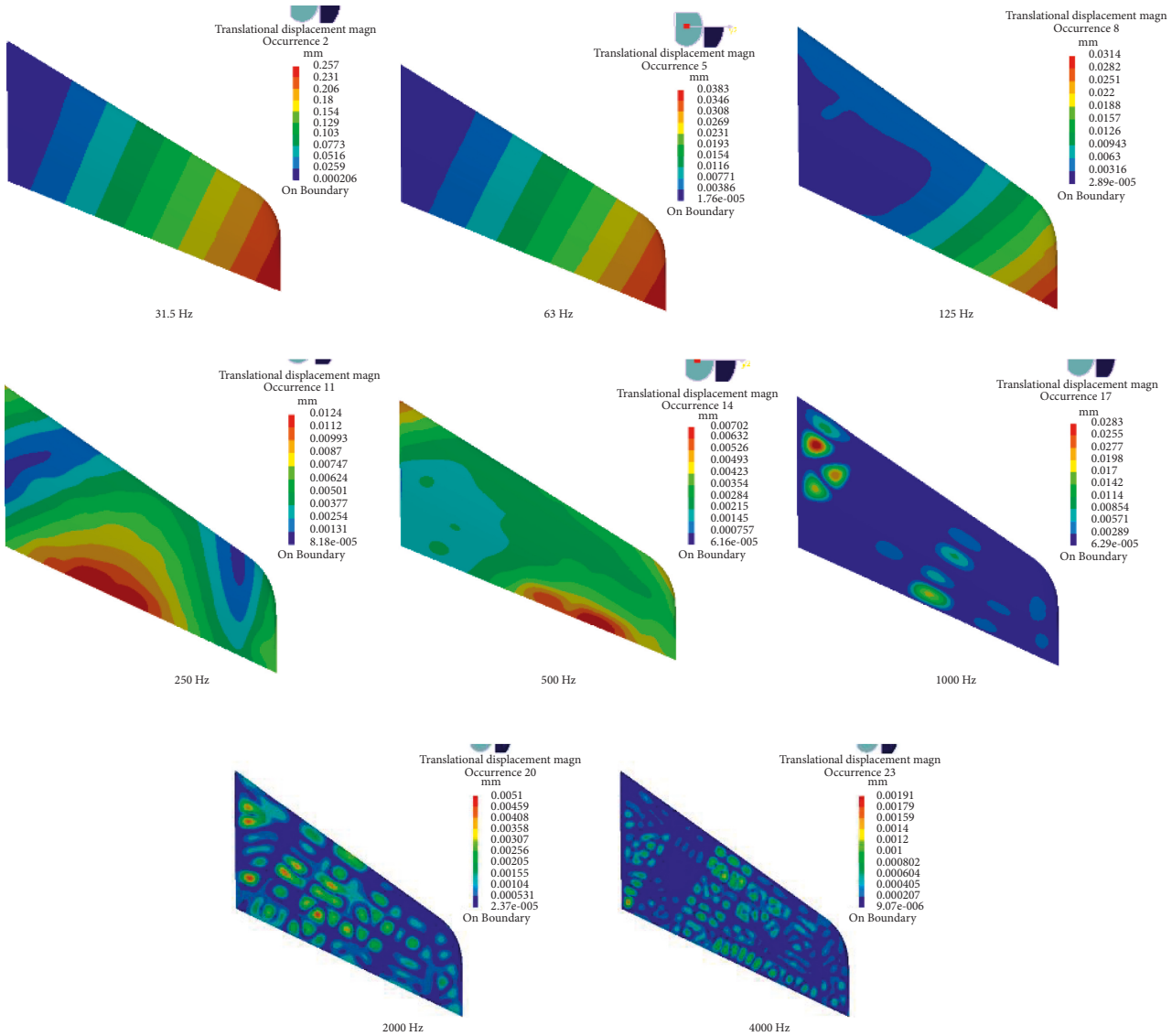

Figure 20: Displacement response.

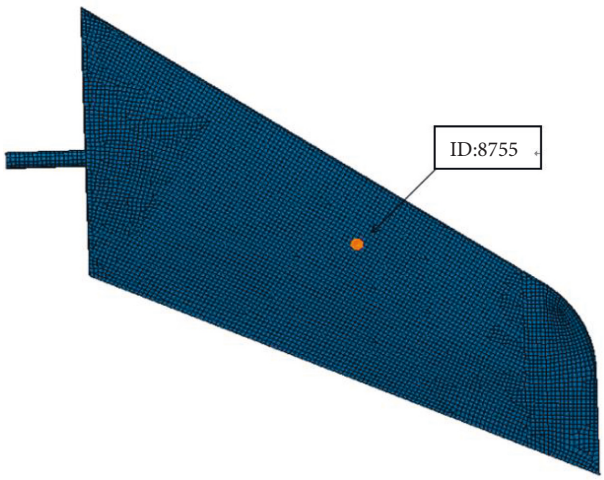

Figure 21: Location of ID 8755.

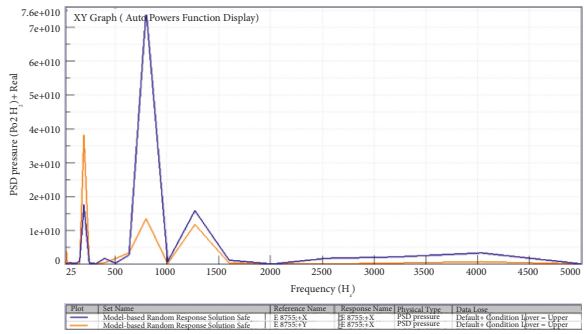

Figure 22: Power spectral density of ID 8755.

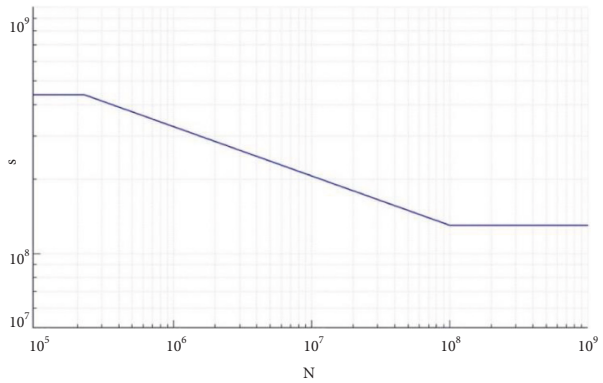

Figure 23: 2A14 S–N curve.

spectral parameters of the response power spectral density. Then, the life is calculated by combining the S–N curve and fatigue cumulative damage theory [22].

The noise signal of the aircraft is high-frequency broadband random signal. The Dirlik model is simple, fast, and suitable for wideband signal. In this study, the Dirlik model is selected, and the Goodman linear formula is used to calculate average stress.

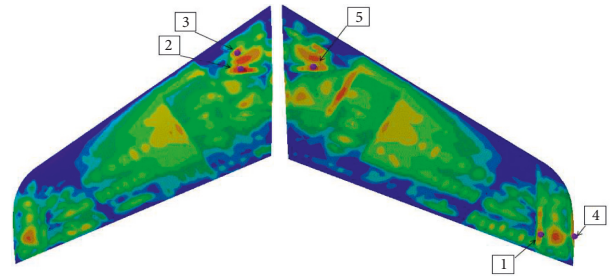

Figure 24: Tail hot spots inside and outside the tail.

Table 5: Hot damage index and life expectancy.

Hot spot	Grid number	Damage index	Fatigue life (s)
1	1212	−3.26	1.83×10^7
2	6951	−3.43	2.70×10^7
3	6974	−3.46	2.89×10^7
4	1630	−3.47	2.97×10^7
5	6796	−3.54	3.51×10^7

4.3. Sound Fatigue Life Results. After determining the stress–life curve of the material, fatigue cumulative damage theory, fatigue life estimation method, and correction method, the external skin of the tail fin is selected as the acoustic fatigue life in Figure 24.

The analysis of Table 5 shows that hot spot 1 is the largest point of damage, and its damage value is $1 \times 10^{-3.26}$ under a standard load. According to the linear fatigue damage accumulation theory, the life under a standard load is $D = 1 \div (1 \times 10^{-3.26}) = 1830$. Since the action time of a standard load is 10000*s*, the vibration fatigue life of hot spot 1 is 1.83×10^7s.

The fatigue risk of the tail is the skin at the root of the tail near the rib and the skin at the wing tip.

The research project has not yet been tested at this stage. Therefore, no test data are compared. To discuss the credibility of the results, the findings are compared with those of the present study. In the study of the estimation of random acoustic fatigue life based on the rain flow counting method, the estimated life of open cylindrical shell is calculated at 140 dB of the total sound pressure level. Jin Luanshan and Li Lin stated that the fatigue life of an aeroengine is calculated on the basis of Dirlik's broadband process theory. Zhang Xiuyi studied the properties of the plate, curved plate, stiffened plate, and honeycomb in the design of the acoustic fatigue analysis and the acoustic fatigue design of the aircraft structure. The calculation results are similar. In this research, the thickness of the aluminum skin is 4.4 mm. Hence, although the load is greater, the sound fatigue life is relatively improved.

5. Influencing Factors of Acoustic Fatigue Life

Theoretically, the factors that affect the cycle fatigue life of the structure also affect the vibration fatigue life, in addition to some factors on the vibration fatigue life of a greater impact, especially the dynamic characteristics of the structure, including natural frequency and damping ratio. The problem of the load on sound fatigue is particular that it needs further study.

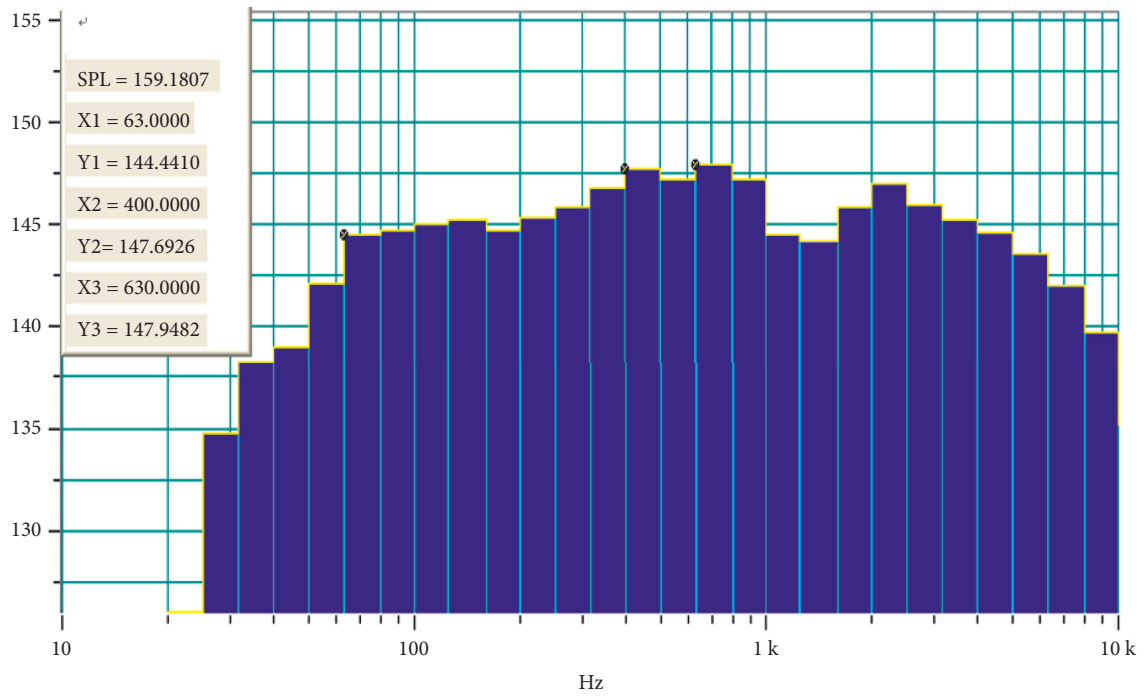

Figure 25: Noise spectrum.

Table 6: Sound pressure spectrum.

Frequency (Hz)	Sound pressure level L_p	Sound pressure spectrum p_e (Pa)
25	134.8	109.9
31.5	138.1	160.7
40	138.8	174.2
50	142.0	251.8
63	144.4	331.9
80	144.6	339.6
100	144.9	351.6
125	145.1	359.8
160	144.4	331.9
200	145.1	359.8
250	146.0	399.1
315	146.5	422.7
400	147.7	485.3
500	146.8	437.6
630	148.0	502.3
800	146.8	437.6
1000	144.0	317.0
1250	144.0	317.0
1600	146.0	399.1
2000	146.8	437.6
2500	146.0	399.1
3150	145.1	359.8
4000	144.4	331.9

5.1. Effects of Load Characteristics. The noise environment of the aircraft at different times varies, and the new noise test data in the new operating conditions are shown in Figure 25. As a result of the use of the 1/3 octave spectrum, the measurement data points likely use the same method in Table 6.

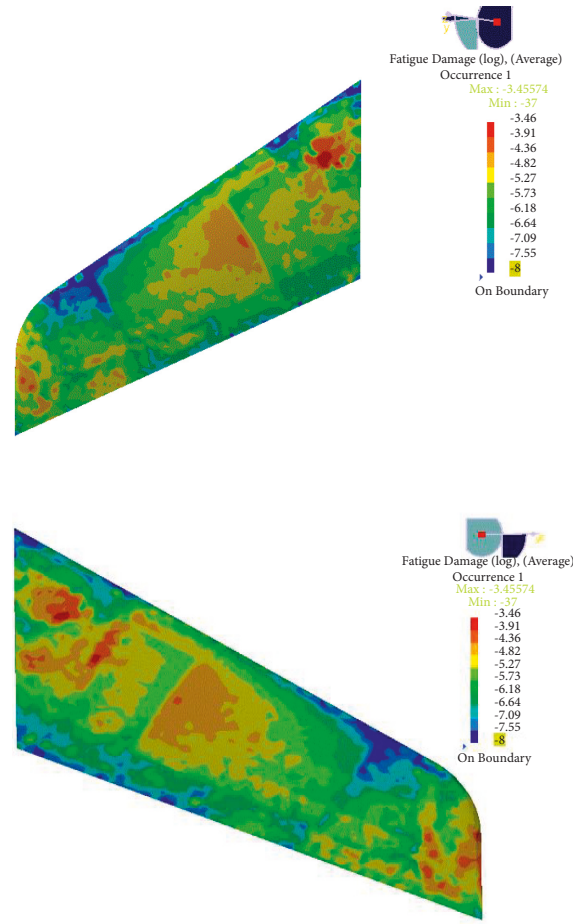

Figure 26: Damage index under 1/3 octave conditions inside and outside tail.

Table 7: Sound fatigue life at different sound pressure levels.

Increase or decrease the value	Damage index	Sound fatigue life
−15	−6.22	$1.65 \times 10^{10} s$
−10	−5.41	$2.58 \times 10^{9} s$
−5	−4.51	$1.78 \times 10^{8} s$
0	−3.26	$1.83 \times 10^{7} s$
+5	−2.45	$2.85 \times 10^{6} s$
+10	−1.51	$3.21 \times 10^{5} s$
+15	−0.33	$2.15 \times 10^{4} s$

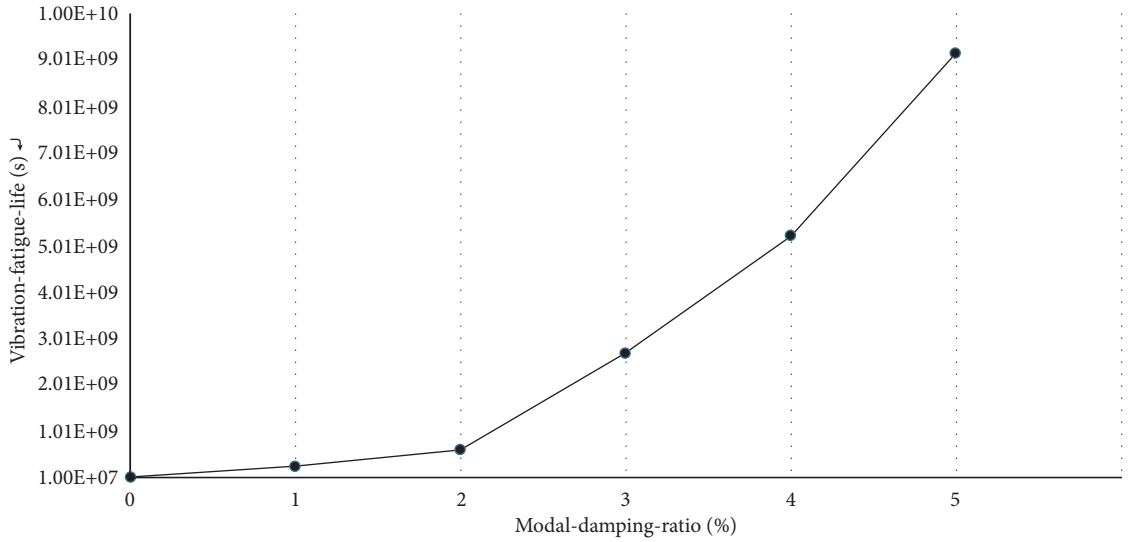

Figure 27: Relationship between vibration fatigue life and modal damping ratio.

Comparing damage index under 1/3 octave conditions inside and outside the tail in Figure 26, we find that (1) parts of the fatigue risk are roughly the same, which are the root near the ribs and the wing at the end of the skin. (2) The fatigue life of the new working condition is increased by an order of magnitude compared with that of the initial working condition. The reasons are that the sound pressure level of the frequency band in the new working condition is smaller than the initial working pressure level, and the external load energy is weakened, thereby increasing life expectancy.

5.2. Relationship between Sound Pressure Level and Life. To obtain the relationship between the external excitation pressure level and the acoustic fatigue life, the sound pressure level of each band is increased and decreased on the basis of the sound pressure load of the original octave. The amplitude of increase or decrease is dB. A new sound pressure spectrum is also obtained.

In Table 7, the analysis of the table data reveals the sound pressure level for each additional 5 dB, and the life expectancy is reduced by about an order of magnitude. For each lower 5 dB, the life is increased by about an order of magnitude. Theoretically, the sound pressure level increases by twice as much as the sound pressure level, and the acoustic energy is proportional to the square of the sound pressure. Therefore, the noise level can reduce the sound fatigue life.

5.3. Effect of Structural Damping. For the modal damping ratio of each order, only the important mode of influence is the main mode; hence, only the main modal damping ratio can be obtained. With the increase of the damping ratio, the ability of the structure to dissipate energy is enhanced, and the structural response caused by the external excitation of the same energy is weakened. Therefore, the fatigue life of the structure increases. The relationship between the damping ratio and the fatigue life can be expressed by a certain function by studying the properties of the material.

Taking different modal damping ratios and performing recalculations to obtain the damage index and the fatigue life, the following is summarized in Table 8.

Figure 27 shows that (1) the modal damping ratio has a great influence on the vibration fatigue life of the structure, and the influence coefficient is nonlinearly increased. (2) With the increase of modal damping, the mean square root of the structural response stress decreases, and the acoustic fatigue life is prolonged.

At present, quantitative research on damping is few. The value of engineering application is usually based on empirical data, which lead to the design damping and the actual damping in many structures. Moreover, the prediction accuracy of vibration fatigue life is not high. To improve the acoustic fatigue life, increasing the structural modal damping is of great significance. The damping materials and

Table 8: Sound fatigue life under different modal damping ratios.

Modal damping ratio (%)	Damage index	Sound fatigue life (s)
0	−3.26	1.83×10^7
1	−4.39	2.45×10^8
2	−4.77	5.93×10^8
3	−5.43	2.68×10^9
4	−5.72	5.22×10^9
5	−5.96	9.15×10^9

shock absorbers are used in the engineering to achieve the purposes of vibration and noise reduction.

6. Conclusion

In this work, the tail fins of a certain type of spacecraft are studied; the finite element, boundary element, and vibration fatigue analysis method are also used to predict the acoustic fatigue life of the tail fins. On this basis, the influence factors of the acoustic fatigue life are investigated, and some suggestions are put forward for the structural fatigue design.

The damage value of largest point is $1 \times 10^{-3.26}$ under a standard load. According to the linear fatigue damage accumulation theory, the life under a standard load is $D = 1 \div (1 \times 10^{-3.26}) = 1830$. Since the action time of a standard load is 10000 s, the vibration fatigue life of hot spot 1 is 1.83×10^7 s. The fatigue risk of the tail is the skin at the root of the tail near the rib and the skin at the wing tip.

The analysis of the table data reveals the sound pressure level for each additional 5 dB, and the life expectancy is reduced by about an order of magnitude. For each lower 5 dB, the life is increased by about an order of magnitude. Theoretically, the sound pressure level increases by twice as much as the sound pressure level, and the acoustic energy is proportional to the square of the sound pressure. Therefore, the noise level can reduce the sound fatigue life.

The FEM of the tail of a hypersonic aircraft is also performed. The modal parameters within 6000 Hz are calculated, and the natural frequency and mode information are calculated. The acoustic response is given to the acoustic response under the given acoustic load, which includes linear damage accumulation theory, the Dirlik model, and the Goodman linear correction model. The analysis method of vibration fatigue life is studied, combined with the results of dynamic analysis and the stress–life curve of the material; the linear damage accumulation theory, Dirlik model, and Goodman straight line correction model are used to calculate the acoustic fatigue life of the tail wing. In addition, the effects of load characteristics and structural damping on acoustic fatigue life are studied.

Data Availability

The modal data used to support the findings of this study were supplied by Fundamental Scientific Research Business Expenses of Central Universities and access can be obtained from the corresponding author upon reqest.

Conflicts of Interest

The authors declare that they have no conflicts of interest.

Acknowledgments

This work was supported by Fundamental Scientific Research Business Expenses of Central Universities (NJ2020024).

References

[1] M. C. Cheng, C. Hsiao, R. J. Shyu, and D. Cheng, "Analysis and test of spacecraft structural response under launch acoustic environment," *12th AIAA/CEAS Aeroacoustics Conference (27th AIAA Aeroacoustics Conference)*, Cambridge, MA, USA, 2006.

[2] D. Priour, "Finite element method," *Dictionary Geotechnical Engineering/wörterbuch Geotechnik*, vol. 73, pp. 3–13, 2013.

[3] S. Kong, S. Zhou, Z. Wang, and K. Wang, "The size-dependent natural frequency of Bernoulli-Euler micro-beams," *International Journal of Engineering Science*, vol. 46, no. 5, pp. 427–437, 2008.

[4] V. Giannella, R. Lombardi, M. M. Pisani, L. Federico, M. Citarella, and R. Citarella, "A novel optimization framework to replicate the vibro-acoustics response of an aircraft fuselage," *Applied Sciences*, vol. 10, no. 7, p. 2473, 2020.

[5] Ji-li Rong and Bo-chao Fan, "Research on scaling characteristics of sound-vibration environment of rocket fairing," *Journal of Astronautics*, vol. 40, no. 8, 2019.

[6] F. E. N. G. Jin-long, H.-hong Wang, Y. Zhao, Yi-nan Wang, and D. U. Li-gang, "Finite element-boundary element method simulation for acoustic-vibration problems of spacecraft structures," *Equipment Environmental Engineering*, vol. 15, no. 11, 2018.

[7] Y. Sha, A. Sise, F. Zhao, and Z. Jiang, "Vibro-acoustic response analysis and fatigue life prediction of thin-walled structures with high speed heat flux," *Acta Aeronautica et Astronautica Sinica*, vol. 41, no. 2, 2020.

[8] J. Xu, Y. Zhang, Q. Han, J. Lacidogna, and G. Lacidogna, "Research on the scope of spectral width parameter of frequency domain methods in random fatigue," *Applied Sciences*, vol. 10, no. 14, p. 4715, 2020.

[9] J. Jang and J. W. Park, "Simplified vibration PSD synthesis method for MIL-STD-810," *Applied Sciences*, vol. 10, no. 2, p. 458, 2020.

[10] A. A. Jaoude and K. El-Tawil, "Analytic and nonlinear prognostic for vehicle suspension systems," *American Journal of Engineering and Applied Sciences*, vol. 6, no. 1, pp. 42–56, 2013.

[11] A. Portela, M. H. Rooke, and D. P. Rooke, "The dual boundary element method: effective implementation for crack problems," *International Journal for Numerical Methods in Engineering*, vol. 33, no. 6, pp. 1269–1287, 1992.

[12] J. T. Chen, K. H. Chen, I. L. Chen, and L. W. Liu, "A new concept of modal participation factor for numerical instability in the dual BEM for exterior acoustics," *Mechanics Research Communications*, vol. 30, no. 2, pp. 161–174, 2003.

[13] P. H. Light and M. C. Light, "Fatigue under wide band random stresses," *Journal of the Structural Division*, vol. 106, no. 7, pp. 1593–1607, 1980.

[14] G. Manogaran, V. Saravanan, and C. H. Hsu, "Information-centric content management framework for software defined internet of vehicles towards application specific services,"

IEEE Transactions on Intelligent Transportation Systems, vol. 22, no. 7, pp. 4541–4549, 2021.

[15] N. W. M. Bishop, *Vibration Fatigue Analysis in Finite Element Environment*, Xvi Encuentro Delgrupo Espanol De Fractura, Torremolinos, Spain, 1999.

[16] P. A. Kumaraswamy, "A generalized probability density function for double-bounded random processes," *Journal of Hydrology*, vol. 46, no. 1-2, pp. 79–88, 1980.

[17] 张. Zhang Lei, 杨. Yang Yang, 高. Gao Jie-chao, and 刘. Liu Xing-yuan, "Study on amplified spontaneous emission properties of EnBOD material," *Chinese Journal of Luminescence*, vol. 36, no. 6, pp. 661–665, 2015.

[18] J. Jian Hua and Z. Hong Lun, *The Experimental Research of Goodman Fatigue Diagram of 09V Steel*, Journal of Shanghai Tiedao University, Shanghai, China, 2000.

[19] O. E. A. Agudelo, C. E. M. Marín, and R. G. Crespo, "Sound measurement and automatic vehicle classification and counting applied to road traffic noise characterization," *Soft Computing*, vol. 25, no. 18, Article ID 12075, 2021.

[20] L. Susmel, R. Lazzarin, and P. Lazzarin, "The mean stress effect on the high-cycle fatigue strength from a multiaxial fatigue point of view," *International Journal of Fatigue*, vol. 27, no. 8, pp. 928–943, 2005.

[21] N. Nguyen, M. C. Leu, and X. F. Liu, "Real-time Communication for Manufacturing Cyber-Physical Systems," in *Proceedings of the 2017 IEEE 16th International Symposium on Network Computing and Applications (NCA)*, pp. 1–4, Cambridge, MA, USA, October 2017.

[22] A. D. Dimarogonas, "Method and apparatus for predicting sturctural integrity by estimating modal damping factor," Patent No. 5 US5652386A, 1997.